Nonlinear elastic imaging using reciprocal time reversal and third order symmetry analysis

Francesco Ciampa and Michele Meo[a)]
Material Research Centre, Department of Mechanical Engineering, University of Bath, Bath, BA2 7AY, United Kingdom

(Received 14 June 2011; revised 25 March 2012; accepted 5 April 2012)

This paper presents a nonlinear imaging method for the detection of the nonlinear signature due to impact damage in complex anisotropic solids with diffuse field conditions. The proposed technique, based on a combination of an inverse filtering approach with phase symmetry analysis and frequency modulated excitation signals, is applied to a number of waveforms containing the nonlinear impulse responses of the medium. Phase symmetry analysis was used to characterize the third order nonlinearity of the structure by exploiting its invariant properties with the phase angle of the input waveforms. Then, a "virtual" reciprocal time reversal imaging process, using only *one broadcasting transducer and one receiving transducer*, was used to insonify the defect taking advantage of multiple linear scattering as mode conversion and boundary reflections. The robustness of this technique was experimentally demonstrated on a damaged sandwich panel, and the nonlinear source, induced by low-velocity impact loading, was retrieved with a high level of accuracy. Its minimal processing requirements make this method a valid alternative to the traditional nonlinear elastic wave spectroscopy techniques for materials showing either classical or non-classical nonlinear behavior. © *2012 Acoustical Society of America*. [http://dx.doi.org/10.1121/1.4707522]

PACS number(s): 43.25.Ed, 43.40.Fz, 43.40.Le [ROC] Pages: 4316–4323

I. INTRODUCTION

Brittleness of composite materials to impact loading limits their use in aerospace, automotive, and marine applications. Indeed, low-velocity impacts can cause delamination beneath the surface, which may appear to be undamaged upon visual inspection. Such a structural defect is called barely visible impact damage (BVID) and it may generate a significant reduction in local strength, thus leading to possible catastrophic failures. Hence, there is a need to develop reliable ultrasonic monitoring techniques capable of localizing and assessing the impact damage.[1,2] The theoretical model of nonlinear interaction of an acoustic/ultrasonic wave with the material defect relies on a first order perturbation power series of the strain associated to the general inhomogeneous partial differential equation (PDE) describing elastic wave motion. Microcracked or undamaged materials that have atomic elasticity (aluminum, steel, Plexiglas) arising from atomic-level forces between atoms and molecules show a classical nonlinear elasticity (CNE).[3] However, the material response in the presence of micro-structural features such as cracks in the medium lattice or delamination may become highly nonlinear and exhibit quasi-static and dynamics nonlinear effects such as hysteresis and relaxation (slow dynamics) in the stress-strain relationship. Such nonlinear effects were also observed in volumetrically damaged materials including rocks, sandstones, ceramics, granular media, and concrete.[4] These nonlinear phenomena are principally due to the *biphasic* structure of such media, known as *nonlinear mesoscopic elastic* (NME), that exhibit a large nonlinear response generated by "hard" viscoelastic grains embedded within "soft" inclusions at mesoscopic level (of the order of one to hundreds μm) termed *bond system* (microcracks, grain contacts, and dislocations). Hence, a new theory was developed by McCall and Guyer[5] to describe not only classical nonlinearity, but also hysteresis and discrete memory effects.

Nonlinear elastic effects of damaged materials can be assessed with *nonlinear elastic wave spectroscopy* (NEWS) techniques, which explicitly interrogate the material nonlinear elastic behavior and its effect on wave propagation caused by the presence of defects.[6–8] One of these methods is based on the nonlinear interaction between two harmonic plane waves having two single frequencies, f_1 and f_2, with $f_1 \ll f_2$ and two different amplitudes A_1 and A_2, with $A_1 \gg A_2$. The material acts as a nonlinear mixer so that when the harmonic waveforms interact together in the same localized damaged region, not only their superposition, but also *sum and difference frequencies*[9] in addition to *higher harmonics*[10] and *subharmonics*[11] of the fundamental frequencies f_1 and f_2, can be generated. These new frequency components indicate that a crack or delamination is present within the material. In terms of strain amplitudes, experimental and numerical evidence showed that the third harmonic amplitude of a hysteretic material is quadratic with the fundamental amplitude, while a cubic dependence is predicted by CNE theory.[12]

In the last few years, NEWS methods have been combined with time reversal acoustics (TRA) techniques in order to focus acoustic energy and illuminate primary (impact points) or secondary sources (scatterers) in a medium regardless of its heterogeneity. TRA is based on the principle of time-reversal invariance and spatial reciprocity of the wave equation in a lossless medium, and it is usually split into two steps. In the *forward propagation* step, the elastic waves diverging from the source are recorded by a set of transducers [time reversal mirror (TRM)]. Then, in the *backward*

a)Author to whom correspondence should be addressed. Electronic mail: m.meo@bath.ac.uk

 0001-4966/2012/131(6)/4316/8/$30.00

propagation step, the acquired waveforms can be focused back to the original excitation point if the output measured by the sensors is time reversed and emitted into the medium.[13] Nevertheless, it was demonstrated by Derode *et al.*[14] that even though TRM of finite bandwidth and aperture limits the focusing quality, the presence of a reverberant diffuse wave field (multiple scattering, mode conversion, and boundary reflections) in a geometrically complex medium (with stiffeners, rivets, holes, and voids) enhances the spatial focusing of the re-emitted signals.[15,16] The effect is to create a virtual enlargement of the transducers angular aperture (kaleidoscopic effect), thus to permit the reduction of the number of sensors needed to back-propagate the acquired waveforms, even to only one single element.[17] However, from the study of the elastodynamic wave equation, time reversal invariance is due to the presence of the even order time partial derivative operator. This condition cannot be satisfied in absorbing media, as the wave equation presents a time partial derivative operator of the first order.[18] Indeed, although spatial reciprocity and TRA invariance hold in diffuse wave fields or anisotropic media, nonlinear attenuation with the wave amplitude breaks the time reversal symmetry. Such aberrations generate phase and amplitude distortions of the propagating wave front, and the behavior of a TRM becomes very difficult to predict. However, Tanter *et al.*[19] showed that the inverse filtering (IF) or reciprocal TRA allows the recovering of the optimal focusing, even in dissipative media.

This paper presents an imaging method aimed to locate the third order nonlinearity in damaged complex anisotropic structures with diffuse field conditions, using only two sensors in pitch-catch mode. The proposed technique is based on a combination of reciprocal TRA and phase symmetry analysis (PSA) with frequency modulation (FM) excitation, in order to obtain the optimal refocusing on the nonlinear scatterer due to the presence of cracks and delamination. The efficiency of this approach is experimentally demonstrated on a dissipative sandwich panel undergone to impact loading, showing that the damage location can be retrieved with a high level of accuracy.

The layout of the paper is as follows. In Sec. II the theoretical and experimental background of this research work is presented. In Sec. III, the imaging technique is theoretically illustrated by introducing phase symmetry analysis and the nonlinear inverse filtering process. Section IV reports the experimental setup while Sec. V shows the results of the nonlinear imaging method. Then, the conclusions of the paper are presented.

II. BACKGROUND

A. Hysteretic behavior in damaged complex composite structures

Damages in complex composite materials such as matrix cracking, fiber debonding, delamination, etc., increase their heterogeneity and the complexity of the structure in terms of alteration between grainy regions and binding medium. Hence, damaged composite laminates may give raise to non-classical nonlinearity wave effects generated by material hysteretic behavior, which is enhanced with the increase of the damaged state. In particular, Meo and Zumpano[20] showed experimentally that damage introduced on a complex composite structure such as a sandwich plate caused a nonlinear non-classical behavior. Such media display NME phenomena that appears to be much like that in rock or concrete, and they can be described[21] by the Preisach-Mayergoyz model as follows:[5,22]

$$\rho\frac{\partial^2 u(x,t)}{\partial t^2} = M_0\left\{\frac{\partial}{\partial x}[1+K(x,t)]e_x\right\},$$
$$K(x,t) = \left[\beta e_x + \delta e_x^2 + \alpha[\Delta e_x + e_x \mathrm{sign}(\dot{e}_x)]\right], \quad (1)$$

where M_0 is the longitudinal elastic modulus, $e_x = \partial u(x,t)/\partial x$ is the strain along the x-direction of propagation of the elastic wave, β and δ are higher order nonlinear elastic coefficients, normally of the order of 1–10 in value, Δe_x is the local strain amplitude over a previous wave period, $\dot{e}_x = \partial e_x/\partial t$ is the strain rate, $\mathrm{sign}(\dot{e}_x) = 1$ if $\dot{e}_x > 0$, $\mathrm{sign}(\dot{e}_x) = -1$ if $\dot{e}_x < 0$, and α is a measure of the material hysteresis. According to Guyer *et al.*[5] and Johnson,[12] experimental and numerical evidence showed the third harmonic amplitude of a purely NME material is quadratic with the fundamental amplitude, while a cubic dependence is predicted by CNE theory. Thus, for NME media third harmonic signature can be chosen to identify the damage as it is the lowest harmonic with the larger energy content predicted by the nonlinear material hysteretic models.[23]

B. Nonlinear imaging with time reversal acoustics

TRA has been widely used for biomedical ultrasound applications, seismology, underwater acoustics, imaging of scatterers for Non-destructive evaluation (NDE),[24] and the identification of the impact sources in solid media.[25] The earliest work on TRA dedicated to localize and characterize scatterers in a multiple scattering medium was carried out by the group at the University of Paris VII (Laboratoire Ondes et Acoustique, ESPCI), who developed three different techniques: ITRM (iterative time reversal method),[26] DORT (decomposition of the time reversal operator),[27] and MUSIC (multiple signal classification scheme) methods.[28] Although ITRM can illuminate only the strongest scatterer present on the medium, both DORT and MUSIC are based on the singular value decomposition (SVD) of the transfer matrix of the structure, which allows extracting for each frequency, a set of N number (singular values) related to the reflectivity of a specific scatterer present in the medium. Then, each singular value is associated to a set of N signals, which are the Fourier transforms of the waveforms used to focus on the singular scatterer.[29] However, such methods were used to localize only linear scatterers as boundary reflections and mode conversion in complex structures. In addition, with these methodologies, the number of transducers must be equal or greater than the number of targets to be illuminated, which limits their use for real NDE applications.

Over the last ten years, much work on NDE techniques with NEWS and TRA has been conducted by Los Alamos National Laboratory, in collaboration with a number of other institutions. A first method, called TREND (time reversal elastic nonlinear diagnostic), was applied to the analysis of

complex superficial cracks in a bounded medium by measuring, with a scanner laser vibrometer, the harmonic/sidebands content of the retro-focusing waveforms after a TRA operation.[30] A second technique employs only the harmonic filtered nonlinear components of narrow frequency band sources, in order to illuminate only nonlinear scatterers, such as microcracks.[31]

Besides these mentioned methods, novel signal processing techniques were associated with TRA in order to enhance the focusing of nonlinearities.[32] Scalerandi *et al.*[33] developed a nonlinear imaging method based on a combination of TRA and scaling subtraction method (SSM). This last technique relies on the analysis of the differences of two received waveforms, one with very low excitation amplitude (approximated to a linear signal) and the other with larger excitation amplitude, linearly scaled. The difference between two waveforms acquired is a signal sum of three contributions that takes into account not only the higher harmonic effects, but also nonlinear attenuation mechanisms and amplitude dependence on the wave speed. These last two phenomena mostly affect the fundamental frequency. Furthermore, TRA was combined to phase inversion (PI) method to improve the extraction of nonlinear response in the recorded waveforms compared to a simple Butterworth filter, and the re-focusing at the nonlinear scatterer location.[34,35] PI, already used in landmine detection,[36] eliminates the linear part and odd nonlinear harmonic contribution, taking into account only the even nonlinear harmonic part (second order nonlinearity). Indeed, the only operation performed in PI is the sum of two excitation signals with same amplitude, but phase-inverted (0 and 180 deg). However, it will be shown that PI method can be considered as a particular case of a general paradigm based on the invariant properties of nonlinear systems called phase symmetry analysis (PSA). Indeed, with this procedure, only the odd harmonic contribution (third order nonlinearity) will be extracted to detect the material damage due to delaminations and cracks.

III. NONLINEAR IMAGING METHOD

Symmetry (or invariance) properties of physical phenomena are widely used for the analysis of nonlinear systems. For instance, the symmetries associated with the infinitesimals of Lie groups can be employed to determine the motion of particles propagating in a medium with non-classical nonlinearity.[37] The invariance properties of Korteweg–de Vries stationary solutions (solitary waves) are used as a signature of the dispersive and nonlinear features of the structure.

This research work presents an imaging technique of the nonlinearity in dissipative complex anisotropic structures by using a combination of PSA with FM excitation and reciprocal TRA. In particular, PSA was employed to characterize the third order nonlinear response of a damaged reverberant anisotropic medium with hysteretic behavior by exploiting its invariant properties with the phase angle ϕ of the swept-coded excitation signals. In other words, this method allows determining the phase angle of the input waveforms in order to discern only the odd nonlinear harmonic part from the received output.

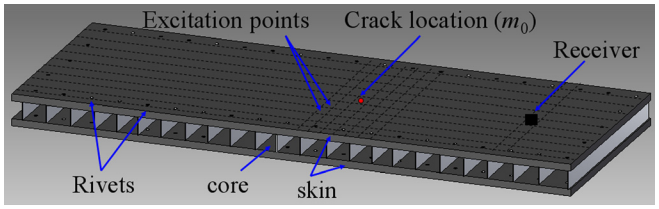

FIG. 1. (Color online) Representation of the sandwich structure with diffuse field conditions.

The imaging process was divided into two steps. In the first step, the third order nonlinear transfer matrices of the structure obtained after PSA process were acquired and stored into the computer memory. Then, exploiting the benefits of multimodal conversion and boundary reflections, known from seismology as *coda*,[38] a "virtual" re-focusing procedure of the recorded signals on the nonlinear source was performed using IF method.

A. Extraction of third order nonlinear impulse response

In the first step, an impact loading was applied to a sandwich composite structure in order to barely indent the medium and to generate delamination localized at the impact site, almost invisible from the top surface (BVID). Then, the damaged zone surrounding the impact point "focusing area" was divided in $M=7\times 6$ "excitation points" distributed along a grid at intervals of 2 cm (Fig. 1). The rest of the sample remains undamaged, so that the nonlinear signature is only present in the region around the defect. In each of the m $(1\le m\le M)$ excitation points a longer duration FM signal with wide frequency bandwidth was transmitted. The swept-coded signal can be expressed in complex notation as

$$x(t)=c(t)e^{j\phi}=e^{j\left[2\pi\left(f_0t+(\mu/2)t^2\right)+\phi\right]},\quad -\frac{T}{2}\le t\le\frac{T}{2},\qquad (2)$$

where f_0 is the central frequency, T is the signal duration (uncompressed pulse width), ϕ is the phase angle, $\mu=B/T$ is the *FM slope*, and B is the total bandwidth that is swept, i.e., the difference between the highest and lowest frequencies within the uncompressed pulse. In our case, $B=$ 70–130 kHz and $T=2$ ms (Fig. 2). Swept-coded signal was chosen in order to improve the signal-to-noise ratio (SNR), the penetration depth, and to keep the sidelobes below the limiting level of the typical dynamical range of an ultrasound image.[39] Then, a

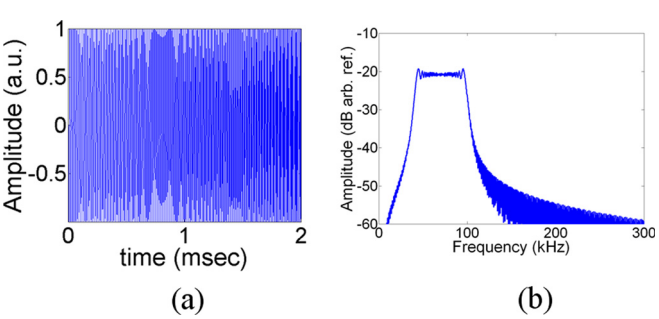

FIG. 2. (Color online) Signal emitted from one of the M excitation points (a) and its spectrum (b).

matched filter (pulse compression) was performed as it allows converting the FM transmitted signal into a band-limited pulse of greater peak power. Indeed, a pulse compression consists of a correlation between the received and the transmitted swept-coded signal. However, the side effects of the matched filter mechanism with linear FM are the resulting *sinc* sidelobes, which represents sources of mutual interference that can obscure weaker signals. Reduction of the compressed pulse range sidelobes was accomplished by shaping the transmitted pulse envelope, i.e., by applying a window function (Blackman) on the matched filter. In this manner, the weighted matched filter is referred to as *mismatched filter* and it is expressed by

$$e(t) = \Im^{-1}[X(\omega)\cdot H_{MF}(\omega)] = e^{j\phi}\frac{1}{2\pi}\int_{-\infty}^{\infty} C(\omega)\cdot H_{MF}(\omega)e^{j\omega t}d\omega \cong \delta(t)e^{j\phi}, \quad (3)$$

where $e_m(t)$ is the new input signal to be time reversed from each excitation point, $C(\omega)$ is the Fourier transform of the transmitted linear FM input function with null phase angle, $H_{MF}(\omega)=W(\omega)C^*(\omega)$, where $W(\omega)$ is the Fourier transform of the window function and the star symbol "*" corresponds to a complex conjugate operation. Compared to a simple pulse compression, the effect of a mismatched filter is to reduce the sidelobes well below the level required for diagnostic imaging. Nevertheless, the undesired effect of a mismatched filtering is to widen the axial main lobe of the output thus slightly decreasing the temporal resolution (although the level is still acceptable) and the SNR improvement of nearly 1 dB.[40]

Assuming that the nonlinear behavior of the medium is described through a third order nonlinear system, the output $f(t)$ received by the sensor placed far from the focusing area can be expressed through a Volterra functional series as follows:[41]

$$\begin{aligned} f(t) &= \sum_{n=1}^{3} f_n(t) = f_1(t) + f_2(t) + f_3(t) \\ &= \int_{-\infty}^{+\infty}\sum_{m=1}^{M}\mathbf{h}_m^{(1)}(\tau_1)\mathbf{e}_m(t-\tau_1)d\tau_1 + \beta\int_{-\infty}^{+\infty}d\tau_1\int_{-\infty}^{+\infty}\sum_{m=1}^{M}\mathbf{h}_m^{(2)}(\tau_1,\tau_2)\mathbf{e}_m(t-\tau_1)\mathbf{e}_m(t-\tau_2)d\tau_2 \\ &\quad + \gamma\int_{-\infty}^{+\infty}d\tau_1\int_{-\infty}^{+\infty}d\tau_2\int_{-\infty}^{+\infty}\sum_{m=1}^{M}\mathbf{h}_m^{(3)}(\tau_1,\tau_2,\tau_3)\mathbf{e}_m(t-\tau_1)\mathbf{e}_m(t-\tau_2)\mathbf{e}_m(t-\tau_3)d\tau_3, \end{aligned} \quad (4)$$

where $\mathbf{e}_m(t)$ is the column vector of the input signal sent by the mth excitation point, $f_1(t), f_2(t), f_3(t)$ are the system partial responses of the linear, second, and third order, respectively, and β and γ are the second and third order nonlinear coefficients, respectively. The nth order kernel of Eq. (4), $\mathbf{h}_m^{(n)}(\tau_1,\ldots,\tau_n)$, is called the *nonlinear impulse response* of order n. This term includes all the nonlinear propagation effects through the medium and the *coda* from the mth excitation point to the receiver.[42] Its Fourier transform is called the *nonlinear transfer function* of order n (the sum term is omitted for clarity reasons)

$$\mathbf{H}_m^{(n)}(\omega_1,\ldots,\omega_n) = \int_{-\infty}^{+\infty}\cdots\int_{-\infty}^{+\infty}\mathbf{h}_m^{(n)}(\tau_1,\ldots,\tau_n) \times e^{-[j(\omega_1\tau_1+\cdots+\omega_n\tau_n)]}d\tau_1\cdots d\tau_n. \quad (5)$$

Since $\mathbf{h}_m^{(n)}(\tau_1,\ldots,\tau_n)$ is a symmetric function of the arguments $(\tau_1,\ldots,\tau_n)$, it follows that $\mathbf{H}_m^{(n)}(\omega_1,\ldots,\omega_n)$ is symmetric for $(\omega_1,\ldots,\omega_n)$. In addition, from the above equation, it can be noted that the usual properties of spectral conjugation still hold

$$\mathbf{H}_m^{(n)*}(\omega_1,\ldots,\omega_n) = \mathbf{H}_m^{(n)}(-\omega_1,\ldots,-\omega_n). \quad (6)$$

However, as the nonlinear impulse response is a function of n variables, the nonlinear system can be simplified by replacing the kernel with its symmetric representation (Wiener model[43]):

$$\mathbf{h}_m^{(n)}(\tau_1,\tau_2,\ldots,\tau_n) = \prod_n \mathbf{h}'^{(n)}_m(\tau), \quad (7)$$

where $\mathbf{h}'^{(n)}_m(\tau)$ is called the sub-kernel of order n. Substituting Eq. (7) into the second and third order nonlinear impulse responses of Eq. (4), we have

$$\begin{cases} \mathbf{h}_m^{(2)}(\tau_1,\tau_2) = \mathbf{h}'^{(2)}_m(\tau_1)\mathbf{h}'^{(2)}_m(\tau_2) \\ \mathbf{h}_m^{(3)}(\tau_1,\tau_2,\tau_3) = \mathbf{h}'^{(3)}_m(\tau_1)\mathbf{h}'^{(3)}_m(\tau_2)\mathbf{h}'^{(3)}_m(\tau_3). \end{cases} \quad (8)$$

Hence, assuming that the impacted point is located at m_0, solving the multiple integrals of Eq. (4), the following terms are obtained:

Linear term

$$f_1(t) = \int_{-\infty}^{+\infty}\mathbf{h}_m^{(1)}(\tau_1)\mathbf{e}_m(t-\tau_1)d\tau_1 = e^{j\phi}\int_{-\infty}^{+\infty}\mathbf{h}_m^{(1)}(\tau_1)\boldsymbol{\delta}_{m0}(t-\tau_1)d\tau_1 = \mathbf{h}_m^{(1)}(t)e^{j\phi}, \quad (9)$$

where $\mathbf{h}_m^{(1)}(t)$ corresponds to the linear impulse response (Green's function) of the structure and $\boldsymbol{\delta}_{m0}$ is a temporal and spatial delta function distribution that is null everywhere, except for $m=m_0$.

Second order term

$$f_2(t) = \beta \int_{-\infty}^{+\infty} d\tau_1 \cdot \int_{-\infty}^{+\infty} \mathbf{h}_m^{(2)}(\tau_1,\tau_2)\mathbf{e}_m(t-\tau_1)\mathbf{e}_m(t-\tau_2)d\tau_2 = \beta \int_{-\infty}^{+\infty} d\tau_1 \cdot \int_{-\infty}^{+\infty} \mathbf{h}'^{(2)}_m(\tau_1)\mathbf{h}'^{(2)}_m(\tau_2)\mathbf{e}_m(t-\tau_1)\mathbf{e}_m(t-\tau_2)d\tau_2$$
$$= \beta e^{j2\phi} \int_{-\infty}^{+\infty} \mathbf{h}'^{(2)}_m(\tau_1)\boldsymbol{\delta}_{m0}(t-\tau_1)d\tau_1 \cdot \int_{-\infty}^{+\infty} \mathbf{h}'^{(2)}_m(\tau_2)\boldsymbol{\delta}_{m0}(t-\tau_2)d\tau_2 = \beta\left[\mathbf{h}'^{(2)}_m(t)\right]^2 e^{j2\phi} = \beta \mathbf{h}_m^{(2)}(t)e^{j2\phi}. \quad (10)$$

Third order term

$$f_3(t) = \gamma \int_{-\infty}^{+\infty} d\tau_1 \cdot \int_{-\infty}^{+\infty} d\tau_2 \cdot \int_{-\infty}^{+\infty} \mathbf{h}_m^{(3)}(\tau_1,\tau_2,\tau_3)\mathbf{e}_m(t-\tau_1)\mathbf{e}_m(t-\tau_2)\mathbf{e}_m(t-\tau_3)d\tau_3$$
$$= \gamma e^{j3\phi} \int_{-\infty}^{+\infty} \mathbf{h}'^{(3)}_m(\tau_1)\boldsymbol{\delta}_{m0}(t-\tau_1)d\tau_1 \cdot \int_{-\infty}^{+\infty} \mathbf{h}'^{(3)}_m(\tau_2)\boldsymbol{\delta}_{m0}(t-\tau_2)d\tau_2 \cdot \int_{-\infty}^{+\infty} \mathbf{h}'^{(3)}_m(\tau_3)\boldsymbol{\delta}_{m0}(t-\tau_3)d\tau_3$$
$$= \gamma\left[\mathbf{h}'^{(3)}_m(t)\right]^3 e^{j3\phi} = \gamma \mathbf{h}_m^{(3)}(t)e^{j3\phi}. \quad (11)$$

Hence, according to Eqs. (9)–(11), Eq. (4) becomes

$$f(t) = \mathbf{h}_m^{(1)}(t)e^{j\phi} + \beta \mathbf{h}_m^{(2)}(t)e^{j2\phi} + \gamma \mathbf{h}_m^{(3)}(t)e^{j3\phi}. \quad (12)$$

Figure 3 illustrates the output recorded by the receiver from one of the mth excitation points in the time domain and its spectrum containing higher harmonics. The results showed that the third order nonlinearity contribution is larger than the second order, highlighting the presence of hysteretic material behavior. Similar results were also experienced in Ref. 17.

Therefore, PSA can be used to eliminate the linear part and the even nonlinear harmonic contribution from the signal acquired by the transducers, by simply imposing the *third order symmetry condition*, $3j\phi = \pm 2\pi kj$, with $k \in \aleph$, where $\aleph$ is the set of all natural numbers. Such an invariant condition is fulfilled for three different phase angles: $\phi = 0$, $\phi = 2/3\pi$, and $\phi = -2/3\pi$. Indeed, PSA consists in sending three phase shifted FM waveforms into the damaged structure, in order to extract only the nonlinear third order signature

$$f_0(t) \underbrace{=}_{\phi=0} \mathbf{h}_m^{(1)}(t) + \beta \mathbf{h}_m^{(2)}(t) + \gamma \mathbf{h}_m^{(3)}(t)$$
$$f_{\frac{2}{3}\pi}(t) \underbrace{=}_{\phi=(2/3)\pi} \mathrm{Re}\left[\mathbf{h}_m^{(1)}(t)e^{j(2/3)\pi} + \beta \mathbf{h}_m^{(2)}(t)e^{j(4/3)\pi} + \gamma \mathbf{h}_m^{(3)}(t)e^{j2\pi}\right] = -\frac{1}{2}\mathbf{h}_m^{(1)}(t) - \frac{\beta}{2}\mathbf{h}_m^{(2)}(t) + \gamma \mathbf{h}_m^{(3)}(t)$$
$$f_{-\frac{2}{3}\pi}(t) \underbrace{=}_{\phi=-(2/3)\pi} \mathrm{Re}\left[\mathbf{h}_m^{(1)}(t)e^{-j(2/3)\pi} + \beta \mathbf{h}_m^{(2)}(t)e^{-j(4/3)\pi} + \gamma \mathbf{h}_m^{(3)}(t)e^{-j2\pi}\right] = -\frac{1}{2}\mathbf{h}_m^{(1)}(t) - \frac{\beta}{2}\mathbf{h}_m^{(2)}(t) + \gamma \mathbf{h}_m^{(3)}(t), \quad (13)$$

where Re[·] indicates that only the real part of the signal was considered for the analysis. Hence, is straightforward that

$$f_{\mathrm{PSA}}(t) = \frac{f_0(t) + f_{(2/3)\pi}(t) + f_{-(2/3)\pi}(t)}{3} = \gamma \mathbf{h}_m^{(3)}(t), \quad (14)$$

where $\mathbf{h}_m^{(3)}(t)$ is the *third order nonlinear impulse response*, and in the angular frequency domain Eq. (14) becomes

$$F_{\mathrm{PSA}}(\omega) = \gamma \mathbf{H}_m^{(3)}(\omega)\mathbf{Y}_{m0}(\omega), \quad (15)$$

where an ideal focusing pattern vector $\mathbf{Y}_{m0}(\omega)$ of length $M \times 1$ was introduced, which corresponds to the signal originating from the defect located at m_0. Its components are $Y_{m0} = 1$ for $m = m_0$, and $Y_{m0} = 0$ for $m \neq m_0$. Figure 4 shows the extraction of the third order nonlinear signature by the sum of the responses coming from the same swept-coded signals sent with different phase angles mentioned previously. For the spatial reciprocity condition, the transpose of

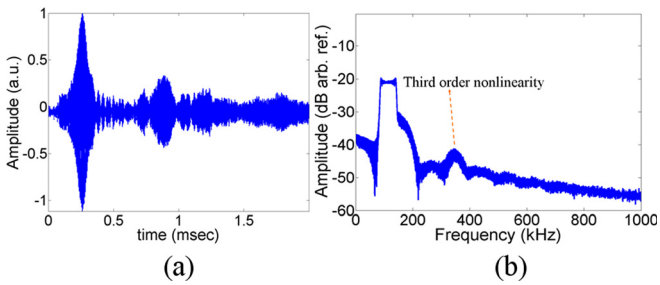

FIG. 3. (Color online) Acquired signal from the mth excitation point (a) and its spectrum containing higher harmonics (b). From this figure it is clearly visible that third order contribution is higher than second order.

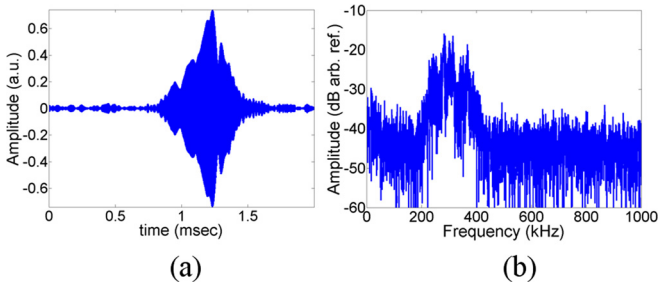

FIG. 4. (Color online) Signal filtered using PSA (a) and its frequency spectrum (b). From (b) it can be clearly seen that only the third order contribution is left .

the third order nonlinear transfer function, $\mathbf{H}_m^{(3)T}(\omega)$, corresponds to the propagation between the receiver and the mth excitation point in the focusing area

$$\mathbf{Y}_{m0}(\omega) = \gamma \mathbf{H}_m^{(3)T}(\omega) F_{\mathrm{PSA}}(\omega). \tag{16}$$

Therefore, the M signals, representing a library containing the third order nonlinear impulse response of the medium from each excitation point to the receiver, were recorded and stored.

B. Nonlinear inverse filtering approach

The second step consists of focusing energy not only at the location of the nonlinearity (m_0), but also to neighboring points (M excitation points). Indeed, the IF method consists of determining the optimal field distribution on the receiver by simply inverting the *third order nonlinear transfer matrix* $\mathbf{H}_m^{(3)}(\omega)$. Such a process would give rise after propagation to the field distribution $\mathbf{Y}_{\mathrm{IF}}(\omega)$ on the focusing plane.[44] Hence, the nonlinear impulse responses stored were digitized over one-bit and broadcast from their original source location to the focusing area. To one-bit a signal, depending on the sign of the recorded signals, the transmitted waveforms were set to ± 1 (the dynamic range limits of the source signal output) in order to increase the amplitude response with a typical gain of approximately 4 dB.[45,46]

The optimal wave field distribution $F_{\mathrm{IF}}(\omega)$ is obtained by multiplying both the left and right sides of Eq. (16) for the complex conjugate of $\mathbf{H}_m^{(3)}(\omega)$ as follows:

$$\begin{aligned}\mathbf{H}_m^{(3)*}(\omega)\mathbf{Y}_{m0}(\omega) &= \mathbf{H}_m^{(3)*}(\omega)\gamma \mathbf{H}_m^{(3)T}(\omega) F_{\mathrm{IF}}(\omega) \\ &= \gamma \left\| \mathbf{H}_m^{(3)}(\omega) \right\|^2 F_{\mathrm{IF}}(\omega),\end{aligned} \tag{17}$$

i.e.,

$$F_{\mathrm{IF}}(\omega) = \frac{1}{\gamma} \tilde{\mathbf{H}}_m^{(3)} \mathbf{Y}_{m0}(\omega), \tag{18}$$

where $\tilde{\mathbf{H}}_m^{(3)} = \mathbf{H}_m^{(3)*}(\omega) / \left\| \mathbf{H}_m^{(3)}(\omega) \right\|^2$ is the inversion of the third order nonlinear operator and $\left\| \mathbf{H}_m^{(3)}(\omega) \right\|^2$ is the squared norm of $\mathbf{H}_m^{(3)}(\omega)$, which represents the square of the third order nonlinear system's modal energy. Such inversion increases the number of modes employed for the back-propagation at the focal point (nonlinear source). Indeed, the modes contained in the signal are weighted by the inverse of the energy at each eigenfrequency. In other words, contributions from modes with weak amplitudes are emitted at higher energies, while contributions from modes with larger amplitudes are back-propagated at lower energies. Hence, with the IF approach, even those modes with weak energy, which are poorly exploited in a simple TRA experiment, can participate in the focusing process.[47]

Therefore, all the waveforms previously acquired (and 1-bit digitized) from the same excitation points processed with PSA, are broadcast into the medium, and the back-propagated signal at the damage location is

$$\begin{aligned}\mathbf{Y}_{\mathrm{IF}}(\omega) &= \lfloor \gamma \mathbf{H}_m^{(3)T}(\omega) \rfloor_{\mathrm{IF}} F_{\mathrm{IF}}(\omega) \\ &= \lfloor \mathbf{H}_m^{(3)T}(\omega) \rfloor_{\mathrm{IF}} \tilde{\mathbf{H}}_m^{(3)}(\omega) \mathbf{Y}_{m0}(\omega),\end{aligned} \tag{19}$$

and the operator $\lfloor \mathbf{H}_m^{(3)T}(\omega) \rfloor_{\mathrm{IF}} \cdot \tilde{\mathbf{H}}_m^{(3)}(\omega)$ is referred to as the third order nonlinear IF operator. The above equation results in a maximum at the focus point (nonlinear scatterer location), i.e., when $m = m_0$. Therefore, the focusing on the nonlinear scattering source can be obtained through a nonlinear "virtual" IF experiment.

IV. EXPERIMENTAL SETUP

The experiments were carried out on a reverberant sandwich plate (750 mm × 405 mm) with rivets (7.9 mm of diameter, Fig. 5). The core used in the sandwich plate was a 6.35 mm thick HRH-10-1/8–4.0 Aramid fiber/phenolic resin nomex (Hexcel, AIM Composites, Cambridge, UK). Facing skins were made of four plies of AS4/8552 unidirectional carbon/epoxy prepreg composite on both sides of the core with lay-up sequence of [90/45/45/90]. A dropped-weight impact test machine with a hemispherical tip was used for hitting the test panel at 12 J. Such energy level was chosen in order to inflict damage in the sandwich panel face sheet corresponding to a BVID. A qualitative image of the defect was obtained through an active pulse thermography, wherein the surface of the sample was actively heated by an external source (a lamp) and the thermal degradation of the heated material was recorded by a high speed infrared (IR) camera.[48] As subsurface temperature decay is governed by

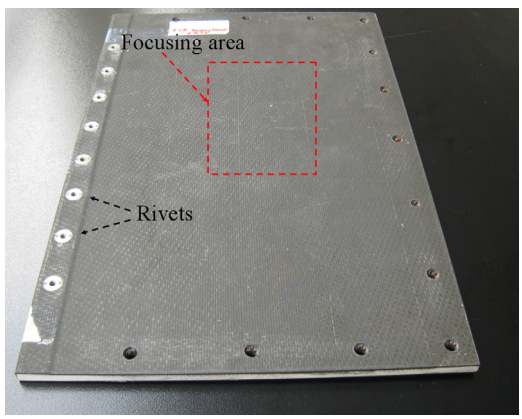

FIG. 5. (Color online) Sandwich test sample used in the experiments.

heat diffusion, retention of heat due to delamination was detected by the camera as a "hot spot" (Fig. 6). Two acoustic emission transducers (20 mm diameter, 10 mm thickness), with a central frequency of 150 kHz, connected to a preamplifier were used to transmit the waveforms from each of the M excitation points ($M = 42$), and to receive the nonlinear elastic responses. In particular, one sensor was instrumented with an oscilloscope (Picoscope 4224, Pico Technology, Eaton Socon, Cambridgeshire, UK) with a sampling rate of 10 MHz. The other acoustic emission (AE) transducer was linked to an arbitrary signal generator (TTi-TGA12104, TTi LTD, Huntingdon, Cambridgeshire, UK) to send the swept-coded signals in the first step and then to send the inverted nonlinear responses into the structure. The frequency band $B = 70$–130 kHz of the FM waveforms was chosen to maximize the efficiency of the available transducers. Moreover, in accordance with the Nyquist theorem, due to the long reverberation present in the signal, a $T = 2$ ms duration time window was chosen. The time histories of the received signals were stored on a computer and processed using a MATLAB software code implemented by the authors.

V. NONLINEAR IMAGING RESULTS

In order to show the feasibility of this "virtual" imaging method, two different cases were analyzed with the receiver sensor placed in two different positions. In case 1, the transducer was positioned at $x_1 = 60$ cm and $y_1 = 17$ cm, while, in case 2, it was located close to the lateral boundary of the sandwich plate with coordinates $x_2 = 4$ cm and $y_2 = 22$ cm. According to Sec. III, the refocusing wave fields at the nonlinear signature location (placed at $x = 38$ cm and $y = 24$ cm) are represented by a normalized two-dimensional (2D) map of the correlation coefficients represented by Eq. (19), and the maxima $\mathbf{Y}_{IF}(\omega)$ in both cases are deduced from the values nearest to 1 (Fig. 7).

The results indicate that a satisfactory image of the defect was obtained in both cases with high accuracy. Moreover, due to very simple signal processing, this method requires very little computational time (lower than 1 s). According to the analytical formulation obtained by Quieffin,[45] the reciprocal TRA technique in reverberant dissipative media is able to increase the contrast, by simply increasing the number of modes participating to the focusing process. In this manner, the effects of distortion (nonlinear attenuation) can be compensated, leading to unambiguous retro-focusing.

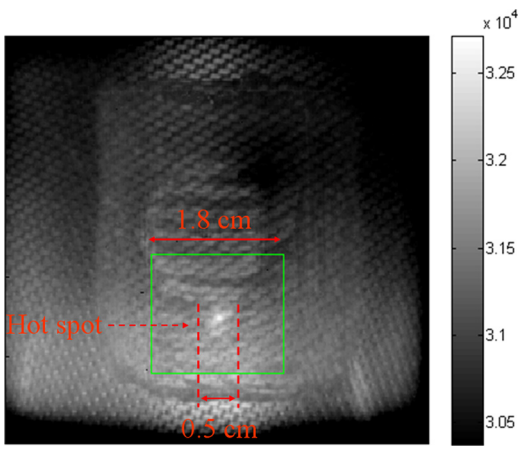

FIG. 6. (Color online) Image of the impacted area obtained through an active pulse thermography. Color bar represents temperature in digit unit.

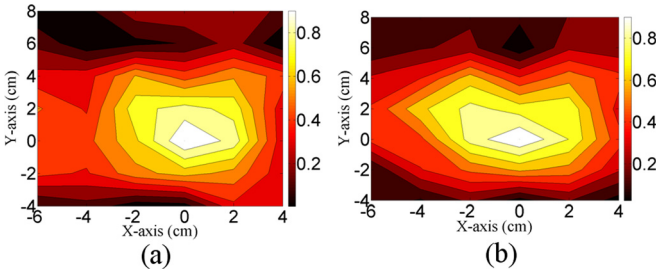

FIG. 7. (Color online) 2D map of the maxima normalized correlation coefficients with the nonlinear imaging method for case 1 (a) and case 2 (b).

Furthermore, from the results obtained in Fig. 7, the following considerations were drawn. First, the focusing can be achieved even when the receiver transducer is close to the boundary of the reverberant sandwich plate (case 2). Such a result demonstrates experimentally that linear scattering from boundary reflections and modes conversion does not influence negatively the "illumination" of the damage, but only carries the information of the nonlinear source to the far field where the sensor is located. Hence, the IF method in combination with the benefits of a diffuse wave field was able to enhance the focusing efficiency (accuracy) to better than the grid spacing of 2 cm, even using one receiver transducer.[21]

In addition, as the nonlinear coefficient γ is not involved in the imaging process [Eq. (19)], compared to other nonlinear TRA techniques,[32] such methodology does not require any normalization with the amplitude of the fundamental frequency. Therefore, in principle, this imaging technique can be applied also for those damages wherein the nonlinearity can be described by classical nonlinear theory. Moreover, for the nonlinear imaging process, no iterative algorithms nor any *a priori* knowledge of the mechanical properties of the medium are required.

VI. CONCLUSIONS

In this paper, an imaging technique of the nonlinear damage signature in a dissipative complex anisotropic structure with hysteretic behavior is reported. The proposed method relies on a combination of phase symmetry analysis with FM excitation and the nonlinear inverse filtering approach, and it was divided into two steps. In the first step, a number of phase shifted waveforms containing the nonlinear impulse responses of the medium were acquired and summed to extract the third order nonlinearity present in the signals due to delaminations and cracks. Then, a "virtual" nonlinear reciprocal time reversal imaging process was employed as it allows achieving the optimal focusing at the nonlinear source by a compensation of the distortion effects in a dissipative medium. Moreover, exploiting the benefits of a diffuse wave field, a high quality localization, with only one sensor and one transmitter, was accomplished. The efficiency of such a technique was experimentally demonstrated on a dissipative sandwich panel undergone to impact loading, and the

nonlinear source was retrieved with a high level of accuracy with little computational time (less than 1 s).

ACKNOWLEDGMENTS

The authors wish to thank Dr. Timothy J. Ulrich from Los Alamos National Laboratory for enlightening discussions and Dr. Simon Pickering and Dr. Umberto Polimeno from the University of Bath for the technical help with the active pulse thermography.

[1]U. Polimeno and M. Meo, "Detecting barely visible impact damage detection on aircraft composites structures," Compos. Struct. **91**(4), 398–402 (2007).
[2]U. Polimeno, M. Meo, D. P. Almond, and S. L. Anfioni, "Detecting low velocity impact damage in composite plate using nonlinear acoustic/ultrasound methods," Appl. Compos. Mater. **17**, 481–488 (2010).
[3]L. Ostrovsky and P.-A. Johnson, "Dynamic nonlinear elasticity in geomaterials," Riv. Nuovo Cimento **24**, 1–46 (2001).
[4]R. A. Guyer and P. A. Johnson., "Nonlinear mesoscopic elasticity: Evidence for a new class of materials," Phys. Today **52**, 30–36 (1999).
[5]R. A. Guyer, K. R. McCall, and G. N. Boitnott, "Hysteresis, discrete memory and nonlinear wave propagation in rock: A new paradigm," Phys. Rev. Lett. **74**, 3491–3494 (1994).
[6]K. E. A. Van Den Abeele, A. Sutin, J. Carmeliet, and P. A. Johnston, "Micro-damage diagnostics using nonlinear elastic wave spectroscopy (NEWS)," NDT&E Int. **34**, 239–248 (2001).
[7]G. Zumpano and M. Meo, "Damage localization using transient non-linear elastic wave spectroscopy on composite structures," Int. J. Non-Linear Mech. **43**(3), 217–230 (2008).
[8]M. Meo, U. Polimeno, and G. Zumpano, "Detecting damage in composite material using nonlinear elastic wave spectroscopy methods," Appl. Compos. Mater. **15**(3), 115–126 (2008).
[9]K. E. A. Van Den Abeele, P. A. Johnston, and A. Sutin, "Nonlinear elastic wave spectroscopy (NEWS) techniques to discern material damage, Part I: Nonlinear wave modulation spectroscopy (NWMS)," Res. Nondestruct. Eval. **12**(1), 17–30 (2000).
[10]J. A. TenCate, E. Smith, and R. A. Guyer, "Universal slow dynamics in granular solids," Phys. Rev. Lett. **85**, 1020–1023 (2000).
[11]A. Moussatov and V. Gusev, "Self-induced hysteresis for nonlinear acoustic waves in cracked material," Phys. Rev. Lett. **90**, 124301 (2003).
[12]P. A. Johnson, "The new wave in acoustic testing," Mater. World **7**, 544–546 (1999).
[13]M. Fink, "Time reversal of ultrasonic fields. I: Basic principles," IEEE Trans. Ultrason. Ferroelectr. Freq. Control **39**(5), 555–566 (1992).
[14]A. Derode, P. Roux, and M. Fink, "Robust acoustic time reversal with high-order multiple scattering," Phys. Rev. Lett. **75**, 4206 (1995).
[15]O. I. Lobkis and R. Weaver, "On the emergence of the Green's function in the correlations of a diffuse field," J. Acoust. Soc. Am. **110**(6), 3011–3017 (2001).
[16]A. Duroux, K. G. Sabra, J. Ayers, and M. Ruzzene, "Extracting guided waves from cross-correlations of elastic diffuse fields: Applications to remote structural health monitoring," J. Acoust. Soc. Am. **127**(1), 204–215 (2010).
[17]C. Draeger and M. Fink, "One-channel time reversal of elastic waves in a chaotic 2D-silicon cavity," Phys. Rev. Lett. **79**, 407 (1997).
[18]M. Tanter, J. L. Thomas, and M. Fink, "Focusing and steering through absorbing and aberrating layers: Application to ultrasonic propagation through the skull," J. Acoust. Soc. Am. **103**(5), 2403–2410 (1998).
[19]M. Tanter, J. L. Thomas, and M. Fink, "Time reversal and the inverse filter," J. Acoust. Soc. Am. **108**(1), 223–234 (2000).
[20]M. Meo and G. Zumpano, "Nonlinear elastic wave spectroscopy identification of impact damage on sandwich plate," Compos. Struct. **71**, 469–474 (2005).
[21]G. Zumpano and M. Meo, "Damage detection in an aircraft foam sandwich panel using nonlinear elastic wave spectroscopy," Comput. Struct. **86**(3–5), 483–490 (2008).
[22]P. A. Johnson, *The Universality of Nonclassical Nonlinearity (with application to Nondestructive Evaluation and Ultrasonics)* (Springer, New York, 2006), Chap. 4, pp. 49–69.
[23]G. Zumpano and M. Meo, "A new nonlinear elastic time reversal acoustic method for the identification and localisation of stress corrosion cracking in welded plate-like structures—A simulation study," Int. J. Solids Struct. **44**, 3666–3684 (2007).
[24]B. E. Anderson, M. Griffa, P.-Y. Le Bas, T. J. Ulrich, and P. A. Johnson, "Experimental implementation of reverse time migration for nondestructive evaluation applications," J. Acoust. Soc. Am. **129**(1), 8–14 (2011).
[25]F. Ciampa and M. Meo, "Impact detection in anisotropic materials using a time reversal approach," Struct. Health Monit. **11**(1), 43–49 (2011).
[26]C. Prada, F. Wu, and M. Fink, "The iterative time reversal mirror: A solution to self focusing in pulse-echo mode," J. Acoust. Soc. Am. **90**, 1119–1129 (1991).
[27]C. Prada, S. Mannevile, D. Spoliansky, and M. Fink, "Decomposition of the time reversal operator: Detection and selective focusing on two scatterers," J. Acoust. Soc. Am. **99**, 2067–2076 (1996).
[28]F. K. Gruber, E. A. Marengo, and A. J. Devaney, "Time-reversal imaging with multiple signal classification considering multiple scattering between the targets," J. Acoust. Soc. Am. **115**(6), 3042–3047 (2004).
[29]E. Barbieri and M. Meo, "Time reversal DORT method applied to nonlinear elastic wave scattering," Wave Motion **47**(7), 452–467 (2010).
[30]T. J. Ulrich, P. A. Johnson, and A. Sutin, "Imaging nonlinear scatterers applying the time reversal mirror," J. Acoust. Soc. Am. **119**(3), 1514–1518 (2006).
[31]T. J. Ulrich, P. A. Johnson, and R. A. Guyer, "Interaction dynamics of elastic waves with a complex nonlinear scatterer through the use of a time reversal mirror," Phys. Rev. Lett. **98**, 104301 (2007).
[32]S. Dos Santos and Z. Prevorovsky, "Imaging of human tooth using ultrasound based chirp-coded nonlinear time reversal acoustics," Ultrasonics **51**, 667–674 (2011).
[33]M. Scalerandi, A. S. Gliozzi, C. L. E. Bruno, D. Masera, and P. Bocca, "A scaling method to enhance detection of a nonlinear elastic response," Appl. Phys. Lett. **92**(10), 101912 (2008).
[34]T. J. Ulrich, A. M. Sutin, T. Claytor, P. Papin, P. Y. Le Bas, and J. A. TenCate, "The time reversed elastic nonlinearity diagnostic applied to evaluation of diffusion bonds," Appl. Phys. Lett. **93**, 151914 (2008).
[35]A. Sutin, B. Libbey, V. Kurtenoks, D. Fenneman, and A. Sarvazyan, "Nonlinear detection of land mines using wide bandwidth time-reversal techniques," Proc. SPIE **6217**, 398–409 (2006).
[36]A. Sutin, B. Libbey, L. Fillinger, and L. Sarvazyan, "Wideband nonlinear time reversal seismo-acoustic method for landmine detection," J. Acoust. Soc. Am. **125**, 1906–1910 (2009).
[37]S. Dos Santos, L. Haumesser, F. Vander Meulen, and O. Bou Matar, "Optimized excitation sources and exact solutions for ultrasonic field propagation in a nonlinear medium with hysteretic behavior," IEEE Trans. Ultrason. Ferroelectr. Freq. Control **2**, 930–933 (2004).
[38]M. Campillo and A. Paul, "Long-range correlations in the diffuse seismic coda," Science **299**, 547–549 (2003).
[39]T. Misaridis and J. A. Jensen, "Use of modulated excitation signals in medical ultrasound. Part I. Basic concepts and expected benefits," IEEE Trans. Ultrason. Ferroelectr. Freq. Control **52**(2), 177–191 (2005).
[40]T. Misaridis and J A. Jensen, "Use of modulated excitation signals in medical ultrasound. Part II. Design and performance for medical imaging applications," IEEE Trans. Ultrason. Ferroelectr. Freq. Control **52**(2), 192–207 (2005).
[41]J. J. Bussang, L. Ehrman, and J. W. Graham, "Analysis of nonlinear systems with multiple inputs," Proc. IEEE **62**, 1088–1119 (1974).
[42]V.-V. Kazakov, A. Sutin, and P.-A. Johnson, "Sensitive imaging of an elastic nonlinear wave-scattering source in a solid," Appl. Phys. Lett. **81**, 646–648 (2002).
[43]W. Greblicki, "Nonparametric approach to Wiener system identification," IEEE Trans. Circuits Syst., I: Fundam. Theory Appl. **44**(6), 538–545 (1997).
[44]F. Ciampa and M. Meo, "Acoustic emission localization in complex dissipative anisotropic structures using a one-channel reciprocal time reversal method," J. Acoust. Soc. Am. **130**(1), 168–175 (2011).
[45]A. Derode, A. Tourin, and M. Fink, "Ultrasonic pulse compression with one bit time reversal through multiple scattering," J. Appl. Phys. **85**(9), 6343–6352 (1999).
[46]G. Montaldo, P. Roux, A. Derode, C. Negreira, and M. Fink, "Generation of very high pressure pulses with 1-bit time reversal in a solid waveguide," J. Acoust. Soc. Am. **110**, 2849–-2857 (2001).
[47]N. Quieffin, "Etude du rayonnement acoustique de structures solides: vers un systeme d' imagerie haute resolution (Study of the acoustic emission of solid structures: towards a high resolution imaging system)," Ph.D. thesis, University Paris VI, France, 2004.
[48]S. Pickering and D. P. Almond, "Matched excitation energy comparison of the pulse and lock-in thermography NDE techniques," NDT & E Int. **41**, 501–509 (2008).